Turbid media optical properties derived from the characteristics of propagating laser radiation beams

**Ljuan Gurdev · Tanja Dreischuh · Orlin Vankov ·
Irina Bliznakova · Lachezar Avramov ·
Dimitar Stoyanov**

Abstract The possibility is studied to develop a straightforward analytical approach to the determination of the optical properties of liquid turbid media having forward-peaked scattering indicatrices. The approach is based on investigating the in-depth behavior of the radius and the axial intensity of a laser radiation beam propagating through the turbid medium. Based on the small-angle approximation, the detected forward-propagating light power spatial distribution, at relatively small or large optical depths along the beam axis, is obtained asymptotically in analytical form allowing one to derive relatively simple expressions of the extinction, reduced-scattering and absorption coefficients and the anisotropy factor of the medium through the characteristics of the propagating light beam. Preliminary experiments have also been performed, using Intralipid dilutions of different relatively low concentrations and measuring the cross-sectional radial distribution of the detected light power at different depths along the beam axis. The corresponding on-axis detected light power profiles have been measured independently as well. The experimental results are consistent with the analytical expressions obtained that allow one to estimate the optical coefficients and the anisotropy factor of the investigated media on the basis of the measured beam characteristics. The values obtained are near those predicted by other researchers.

L. Gurdev (✉) · T. Dreischuh · O. Vankov · I. Bliznakova ·
L. Avramov · D. Stoyanov
Institute of Electronics, Bulgarian Academy of Sciences,
72 Tzarigradsko Chaussee Blvd., 1784 Sofia, Bulgaria
e-mail: lugurdev@ie.bas.bg

1 Introduction

Optical tomography is a hopeful contemporary investigation area that is expected to provide effective noninvasive and ionizing-radiation-free methods and instruments for early diagnosis of serious human tissue diseases. The investigations on numerous variants of optical tomography being developed at present (e.g., [1–6] and references therein) require the knowledge of the optical properties of tissues and tissue-like phantoms and the laws governing the radiative transfer within the investigated biological and mimic objects. The main optical characteristics specifying the normal and abnormal tissues and conditioning the radiative transfer are the integral scattering α_s and reduced scattering $\alpha_{rs} = \alpha_s(1 - g)$ coefficients, the absorption coefficient α_a, the total extinction coefficient $\alpha_t = \alpha_s + \alpha_a$, the scattering indicatrix, and the anisotropy factor g, also called the g-factor [7, 8]. The coefficients α_s, α_a, and α_t of a medium of interest describe, respectively, the scattered, absorbed, and scattered plus absorbed light powers per unit volume of the medium, per unit incident light irradiance. They characterize as well the attenuation, due to scattering, absorption or both, respectively, of a light beam of unit power, per unit length along the direction of its propagation [8]. The scattering indicatrix $i(\vec{s}, \vec{s}')$ describes the probability that a photon propagating in direction $\vec{s}'$ is scattered at angle θ, within unit solid angle around the direction $\vec{s}$; $\vec{s}'$ and $\vec{s}$ are dimensionless directional unit vectors, and $\theta = \arccos(\vec{s} \cdot \vec{s}')$. The scattering anisotropy factor g is defined as the average cosine of the scattering angle θ, obtained by using the indicatrix of the medium (see below). The mean free path (MFP) of a photon in a scattering and absorbing medium, before undergoing scattering or absorption, is $\mathrm{MFP} = \alpha_t^{-1}$. For optical radiation with

wavelength λ from 400 to 1,100 nm, the biological tissues are turbid media characterized by strong scattering and considerably weaker absorption. That is, $\alpha_t \approx \alpha_s \gg \alpha_a$. Then, the mean free path of a photon in tissue will be determined in practice by α_s, i.e., $\mathrm{MFP} = \alpha_t^{-1} \approx \alpha_s^{-1}$. The value of the MFP in this case is usually less than 1 mm, which means that the multiple scattering effects will be essential and the radiative transfer equation should be used for quantitative analysis.

The experimental investigation in vivo of the optical properties of tissues may involve tedious and complicated procedures. Therefore, tissue-simulating phantoms are frequently used for the development, testing, and calibration of novel diagnostic methods and instruments. Certainly, the optical and structural properties of the mimic objects should be like those of tissues. There exist various methods for measuring the optical characteristics of turbid media [9, 10, and references therein]. However, despite the efforts of achieving high measurement accuracy, certain dispersion exists of the results obtained [9, 10]. Therefore, it is expedient to develop various approaches to investigating the radiative transfer in turbid media and mutually validating the experimental results about their optical properties.

A purpose of the present study is to obtain and develop general analytical expressions and procedures for the determination of the optical parameters of a turbid medium through the characteristics of a forward-propagating laser radiation beam. The information characteristics of interest in this case are the on-axis detected power of the forward-propagating light and the beam radius at different depths along the beam axis. So, one would be able to estimate in a straightforward way the optical properties of the medium on the basis of experimental data about the spatial distribution of the detected forward-propagating light power. We suppose that such an aim is attainable by using the potential of the so-called small-angle approach to solving the radiative transfer equation [7, 11–18]. In this case, comparatively simple approximate analytical description can be achieved, for relatively large or small "optical depths," of the transverse radial distribution and the axial in-depth profile of the detected power of the laser radiation beam. The asymptotic approaches, developed and analyzed in detail here, to deriving analytical expressions of the transversal radial distribution and the axial in-depth profile of the detected light power have first been briefly reported in Refs. [19–21]. Initial formulae have also been obtained and used there for estimation of the optical constants of turbid media.

The small-angle approximation should be valid to determinate depths along the beam axis, depending on the turbidity of the medium under investigation and the "sharpness" of its scattering indicatrix. Therefore, the estimation of the in-depth range of validity of this approximation is also an important problem to be considered in the work.

Another important aim of the work is to study experimentally the propagation of laser beams through homogeneous liquid tissue-like media and to determine the cross-sectional radial distribution of the detected forward-propagating light power at different depths along the beam axis as well as the on-axis detected light power profile. In this way, the optical characteristics of the investigated media and the ranges of validity of the small-angle approximation could be estimated experimentally. The early experiments of this type, performed using a progressively upgraded experimental arrangement, are described in [19–21]. It is shown there, in particular, that the total extinction coefficient of relatively low-turbidity media increases linearly with the concentration of scatterers in the medium. Similar in a sense, thorough and precise experiments have been conducted in works [22, 23], where the experimental results are interpreted on the basis of results obtained by Monte Carlo simulations and few scattering and diffusion theoretical approaches.

In the following Sect. 2, analytical expressions are derived in small-angle approximation of the spatial distribution of the detected forward-propagating laser light power for Gaussian and Henyey–Greenstein scattering indicatrices. It is shown as well that the expressions obtained allow one in principle to readily estimate α_t, α_a, α_s, α_{rs}, and g, through experimentally measurable quantities, the on-axis detected light power, and the e^{-1} radius of the forward-propagating light beam at different depths along the beam axis. The experimental setup and procedures are described in Sect. 3. The analysis of the experimental data, from point of view of the analytical results obtained in Sect. 2, is conducted in Sect. 4. In this section, estimation is also performed of the medium characteristics α_t, α_{rs}, and g for both the indicatrices of concern here. A comparison is conducted and discussed as well of the results obtained here with results obtained by other researchers. At last, in Sect. 5, the main conclusions are summarized following from the results obtained in the work. Mathematical details concerning the case of Henyey–Greenstein indicatrix and the validity limits of the small-angle approach are given in Appendices 1 and 2, respectively. Also, an analytical expression of the forward-propagating light radiance is derived and discussed for completeness in Appendix 3.

2 Expressions of the detected forward-propagating laser light power in small-angle approximation

2.1 Stationary radiative transfer equation and detected forward-propagating light power

For a stationary monochromatic radiation field inside a homogeneous and isotropic turbid medium without internal

light sources, the radiative transfer equation has the form [7]:

$$\vec{s} \cdot \text{grad}I(\vec{r};\vec{s}) = -\alpha_t I(\vec{r};\vec{s}) + \alpha_s \int_{4\pi} i(\vec{s},\vec{s}')I(\vec{r};\vec{s}')d\omega', \quad (1)$$

where $I(\vec{r};\vec{s})$ (W m^{-2} sr^{-1}) is the radiance depending in general on the vector coordinate $\vec{r} = \{x,y,z\}$ and the directional unit vector $s = \{s_x, s_y, s_z\}(s_x^2 + s_y^2 + s_z^2 = 1)$; $i(\vec{s},\vec{s}')$ is the scattering indicatrix from a direction $\vec{s}'$ to the direction $\vec{s}$, $\int_{4\pi} i(\vec{s},\vec{s}')d\omega' = 1$, and $d\omega'$ is a differential element of solid angle; and $\alpha_t = \alpha_a + \alpha_s$ (m^{-1}) is the total extinction (linear attenuation) coefficient in the medium, consisting of two components, the integral scattering coefficient α_s and the absorption coefficient α_a.

The turbid medium of interest is assumed to occupy the semi-infinite space $z > 0$; the axis $0z$ of the coordinate frame is chosen to coincide with that of the incident laser beam, and the plane $z = 0$ is identified with the internal entry wall of the experimental plexiglass container filled with liquid turbid medium (Fig. 1). The task to be solved here based on Eq. (1) is first to determine analytically the radiance $I(\vec{r};\vec{s})$ of the forward-propagating laser light (for $s_z > 0$) inside the medium. Then, an analytical expression should be obtained of the light power

$$J(\vec{\rho}, z) = \int_A d\vec{\rho}' \int_{2\pi+} d\omega R(\vec{\rho} - \vec{\rho}';\vec{s})I(\vec{\rho}', z;\vec{s}) \quad (2)$$

detected by a circular optical receiver oriented antiparallel to the beam axis; $\vec{\rho} = \{x,y\}$, $\vec{\rho}' = \{x',y'\}$, $R(\vec{\rho};\vec{s})$ is the receiver directional and aperture-transmittance diagram, A is the receiver aperture area, and $2\pi+$ denotes integration over the positive unit hemisphere. A way of analyzing the radiation transport Eq. (1), concerning the propagation of optical beams in turbid tissue-like media with sharply forward-directed indicatrices [24–26], is the so-called small-angle approximation or approximation of large particles [7, 11–18]. It allows one, under some reasonable

assumptions, to obtain analytical results for $I(\vec{r};\vec{s})$ and finally $J(\vec{\rho}, z)$ ensuring relatively simple determination of the optical properties of a medium of interest.

2.2 Scattering indicatrices

We shall suppose here that the indicatrices of the investigated turbid media have one of the following Gaussian or Henyey–Greenstein [7, 27] forms:

$$i_G(\vec{s},\vec{s}') \cong i_G(|\vec{s}_\perp - \vec{s}'_\perp|)$$
$$= [2\pi(1-g)]^{-1} \exp[-(\vec{s}_\perp - \vec{s}'_\perp)^2/2(1-g)], \quad (3)$$

$$i_{HG}(\vec{s},\vec{s}') = i_{HG}(\mu) = [(1-g^2)/4\pi](1+g^2-2g\mu)^{-3/2}, \quad (4)$$

where $\vec{s}_\perp = \{s_x, s_y\}$, $\vec{s}'_\perp = \{s'_x, s'_y\}$, $|\cdot|$ denotes module, $\mu = \vec{s} \cdot \vec{s}' = \cos\theta$, $\theta \cong |\vec{s} - \vec{s}'| \cong |\vec{s}_\perp - \vec{s}'_\perp| < 1$ is scattering angle, and the anisotropy factor $g = g_{HG} = \int_{4\pi} \mu\, i_{HG}(\mu)d\omega'$ in the latter case, and $g = g_G \cong \int_0^\infty [1 - s_\perp^2/2]\, i_G(\vec{s}_\perp)d\vec{s}_\perp$ in the former case; $s_\perp = |\vec{s}_\perp|$, and $d\vec{s}_\perp = ds_x ds_y$.

2.3 Incident laser beam

The incident laser beam is considered as a collimated Gaussian beam with field amplitude distribution

$$u(\vec{\rho}, z = 0) = u_0 \exp(-\rho^2/2w^2), \quad (5)$$

where w is the initial beam radius, and $u_0 = u(\rho = 0)$ is the initial on-axis field amplitude. The corresponding radiance distribution $I_0(\vec{\rho};\vec{s}_\perp) = I(\vec{\rho}; z = 0;\vec{s}_\perp)$ is then given by [7]

$$I_0(\vec{\rho};\vec{s}_\perp) = (k^2 w^2 I_0/\pi) \exp(-\rho^2/w^2 - k^2 w^2 s_\perp^2), \quad (6)$$

where $k = 2\pi/\lambda$, $I_0 = |u_0|^2$, $\rho = |\vec{\rho}|$, and $P_t = \pi w^2 I_0$ is the total beam power. The radial cross-sectional intensity distribution of the laser beam used in the experiments has a Gaussian shape on the average [20].

Fig. 1 Block-scheme of the experimental setup
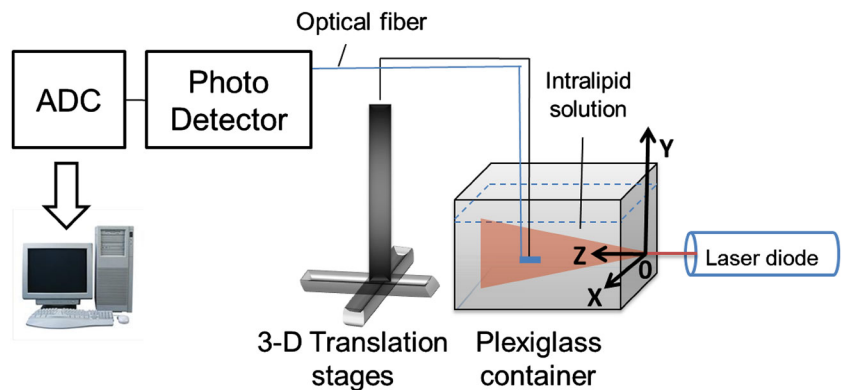
2.4 Directional and aperture-transmittance diagram of the receiver

It is expedient to assume that the receiving optical system has a Gaussian aperture-transmittance and directional diagram with characteristic aperture radius E and angle of view γ, such that

$$R(\vec{\rho}; \vec{s}_\perp) = T \exp\left(-\rho^2/E^2 - s_\perp^2/\gamma^2\right), \tag{7}$$

where $T < 1$ is the central normal-incidence aperture transmittance, at $\rho = 0$ and $s_\perp = 0$. As it is shown in [20], the experimentally determined directional diagram of the optical fiber employed in the measurements is well approximated by a Gaussian curve.

2.5 General expression of $J(\vec{\rho}, z)$ in small-angle approximation

The small-angle approach to solve Eq. (1) is described in detail in [7]. It is based on the possibility of simplifying the radiative transfer equation and using Fourier-transformation technique to obtain the following general result for $I(\vec{r}; \vec{s})$:

$$I(\vec{r}; \vec{s}) = I(\vec{\rho}, z; \vec{s}_\perp)$$
$$= (2\pi)^{-4} \int\limits_{-\infty}^{+\infty} \int d\vec{\kappa} d\vec{q} \exp(-j\vec{\kappa} \cdot \vec{\rho} - j\vec{s}_\perp \cdot \vec{q}) \tilde{I}_0(\vec{\kappa}; \vec{q} + \vec{\kappa}z) K(z; \vec{\kappa}; \vec{q}), \tag{8}$$

where

$$\tilde{I}_0(\vec{\kappa}; \vec{q}) = \int\limits_{-\infty}^{+\infty} \int d\vec{\rho} d\vec{s}_\perp I_0(\vec{\rho}, \vec{s}_\perp) \exp(j\vec{\kappa} \cdot \vec{\rho} + j\vec{s}_\perp \cdot \vec{q}), \tag{8a}$$

$$K(z; \vec{\kappa}; \vec{q}) = \exp\left\{-\alpha_t \int\limits_0^z dz'[1 - W_0 \tilde{i}(\vec{q} + \vec{\kappa}z')]\right\}, \tag{8b}$$

$$\tilde{i}(\vec{q}) = \int\limits_{-\infty}^{+\infty} d\vec{s}_\perp i(\vec{s}_\perp) \exp(j\vec{s}_\perp \cdot \vec{q}), \tag{8c}$$

$W_0 = \alpha_s/\alpha_t$ may be considered as "unity volume albedo" of the turbid medium, j is imaginary unity, $\vec{\kappa} = \{\kappa_x, \kappa_y\}$, $\vec{q} = \{q_x, q_y\}$, $d\vec{\kappa} = d\kappa_x d\kappa_y$, and $d\vec{q} = dq_x dq_y$. The analytical expression of $I(\vec{r}; \vec{s})$ for Gaussian indicatrix and developed scattering ($\alpha_s z \gg 1$), derived using Eqs. (3), (6), and (8–8c), is given and briefly discussed for completeness in Appendix 3.

On the basis of Eqs. (2) and (6–8b), we obtain the following expression of $J(\vec{\rho}, z)$:

$$J(\vec{\rho}, z) = \left(16\pi^2\right)^{-1} TP_t \gamma^2 E^2 \int\limits_{-\infty}^{+\infty} \int d\vec{\kappa} \, d\vec{q}$$
$$\times \exp\left\{-j\vec{\kappa} \cdot \vec{\rho} - \frac{\kappa^2}{4}\left(w^2 + E^2 + \frac{z^2}{k^2 w^2}\right)\right.$$
$$-\frac{q^2}{4}\left(\frac{1}{k^2 w^2} + \gamma^2\right) - \frac{\vec{q} \cdot \vec{\kappa} z}{2k^2 w^2}$$
$$\left. -\alpha_t \int\limits_0^z dz'[1 - W_0 \tilde{i}(\vec{q} + \vec{\kappa}z')]\right\}; \tag{9}$$

$$\kappa^2 = |\vec{\kappa}|^2 = \kappa_x^2 + \kappa_y^2, \quad \text{and} \quad q^2 = |\vec{q}|^2 = q_x^2 + q_y^2.$$

2.6 Expressions of $J(\vec{\rho}, z)$ and estimation of the optical parameters for Gaussian indicatrix

According to Eqs. (3) and (8c), for Gaussian indicatrix

$$\tilde{i}(\vec{q} + \vec{\kappa}z') = \exp[-(1 - g)(\vec{q} + \vec{\kappa}z')^2/2]. \tag{10a}$$

With this expression of $\tilde{i}$, the integrals in Eq. (9) can be estimated analytically for large and small optical depths $\alpha_s z$, when $\alpha_s z \gg 1$ (region of developed scattering) and $\alpha_s z$ is of the order of unity or smaller (region of low scattering), respectively. The depths z within the developed-scattering region exceed essentially the mean free path of the photon, MFP $\approx \alpha_s^{-1}$, between two successive acts of scattering, in practice. That is, $z \gg \alpha_s^{-1}$. Consequently, the light undergone multiple scattering is prevailing in this region. At the same time, the depths z within the low-scattering region are less or of the order of α_s^{-1}. Therefore, in this region, the forward-propagating light consists mainly of two components, unscattered and single-scattered light.

In the region of developed scattering ($\alpha_s z \gg 1$), the integrand contributes to the integral only within a narrow domain of values of $\vec{q}$ and $\vec{\kappa}z'$, where $|\vec{q} + \vec{\kappa}z'| \ll 1$. Out of this domain, the integrand function sharply tends to zero with the increase of q and/or $\vec{\kappa}z'$. Then, the indicatrix spectrum $\tilde{i}(\vec{q} + \vec{\kappa}z')$ in Eq. (9) may be expanded in exponential series, retaining only the first two terms, that is,

$$\tilde{i}(\vec{q} + \vec{\kappa}z') = 1 - (1 - g)(\vec{q} + \vec{\kappa}z')^2/2. \tag{10b}$$

Using this asymptotic representation of $\tilde{i}$ in Eq. (9), after straightforward but cumbersome integration, we obtain that

$$J(\vec{\rho}, z) = P_t TE^2 \gamma^2 Q^{-1}(\chi z, z, \gamma) \exp\{-\rho^2/w^2(z) - \alpha_a z\}, \tag{11}$$

where $\chi = \alpha_{rs}$,

$$w(z) = [Q(\chi z, z, \gamma)/P(\chi z, z, \gamma)]^{1/2} \tag{12}$$

is the e^{-1} half-width of the beam at a distance z,

$$Q(\chi z, z, \gamma) = (w^2 + E^2)(k^{-2}w^{-2} + \gamma^2 + 2\chi z) + z^2\gamma^2 k^{-2}w^{-2}$$
$$+ (2/3)\chi z^3(k^{-2}w^{-2} + \gamma^2) + (1/3)\chi^2 z^4$$
$$\cong (1/3)\chi z^3(2\gamma^2 + \chi z), \tag{13}$$

and

$$P(\chi z, z, \gamma) = [Q(\chi z, z, \gamma) + \chi^2 z^4]/(w^2 + E^2 + 2\chi z^3/3)$$
$$\cong \gamma^2 + 2\chi z. \tag{14}$$

The approximate expressions of Q and P are obtained, taking into account that $k^{-2}w^{-2} \ll 1$, and $(z/kw) \ll w, E \ll z$. When the angle of view of the receiver is small enough, such that $\gamma^2 \ll \chi z$, from Eqs. (11)–(14), we obtain

$$J(\vec{\rho}, z) = (3P_t TE^2\gamma^2/\chi^2)z^{-4}\exp\{-\rho^2/w^2(z) - \alpha_a z\}, \tag{15}$$

and

$$w^2(z) \cong \chi z^3/6. \tag{16}$$

In the opposite case ($\gamma^2 \gg \chi z$),

$$J(\vec{\rho}, z) = (3P_t TE^2/2\chi)z^{-3}\exp(-\rho^2/w^2(z) - \alpha_a z), \tag{17}$$

and

$$w^2(z) \cong (2/3)\chi z^3. \tag{18}$$

Expressions (17) and (18) are in accordance with the corresponding results obtained, e.g., in Ref. [14], using other, small-angle diffusion approach and other definition of $w^2(z)$, and implying a maximum angle of acceptance $\gamma = \pi/2$. From Eqs. (16) and (18), for the reduced-scattering coefficient $\alpha_{rs} = \chi$, we obtain, respectively,

$$\alpha_{rs} = \chi = 6w^2(z)/z^3, \tag{19}$$

in the former case, and

coefficient α_a is obtainable, respectively, by exponential or log-linear fit of the dependences

$$y_1(z) = J(\vec{0}, z)z^4, \tag{21}$$

in the first case, and

$$y_2(z) = J(\vec{0}, z)z^3, \tag{22}$$

in the second case, where $J(\vec{0}, z)$ is the on-axis detected light power. Thus, the values of the characteristic optical parameters α_{rs} and α_a could be estimated in principle by measuring the on-axis and the transversal radial distributions of the detected light power. Then, provided that the extinction coefficient α_t is known, the values of the scattering coefficient and the anisotropy factor are obtainable, respectively, as

$$\alpha_s = \alpha_t - \alpha_a, \ g = 1 - \alpha_{rs}/\alpha_s. \tag{23}$$

The value of α_t is determinable by measuring and investigating the behavior of $J(\vec{0}, z)$ in the low-scattering region.

In the region of low scattering, where $\alpha_s z$ is less or of the order of unity, in Eq. (9), the exponential factor containing integral of $\tilde{i}(\vec{q} + \vec{\kappa}z')$ may be expanded in exponential series, retaining only the first two terms. Then, having Eq. (10a) in mind, for the detected power $J(\vec{0}, z)$, we obtain

$$J(\vec{0}, z) = J_b(\vec{0}, z)\exp(-\alpha_t z)[1 + \delta(z, \alpha_s, w, \gamma, g)], \tag{24}$$

where

$$J_b(\vec{0}, z) = P_t T\gamma^2 E^2/[(w^2 + E^2)(k^{-2}w^{-2} + \gamma^2)$$
$$+ z^2\gamma^2 k^{-2}w^{-2}]$$
$$\approx J_b = P_t TE^2/(w^2 + E^2) \tag{24a}$$

is the on-axis detected power of the laser beam unperturbed by absorption and scattering, and

$$\delta(z, \alpha_s, w, \gamma, g) = [16\pi^2 J_b(\vec{0}, z)]^{-1} TP_t\gamma^2 E^2\alpha_s \int_0^z dz' \int_{-\infty}^{+\infty}\int d\vec{\kappa}\,d\vec{q}\,\exp\left\{-\frac{\kappa^2}{4}\left[w^2 + E^2 + z^2 k^{-2}w^{-2} + 2(1-g)z'^2\right]\right.$$
$$\left. - \frac{q^2}{4}\left[k^{-2}w^{-2} + \gamma^2 + 2(1-g)\right] - (\vec{q}\cdot\vec{\kappa}/2)\left[zk^{-2}w^{-2} + 2(1-g)z'\right]\right\} \tag{24b}$$

$$\alpha_{rs} = 3w^2(z)/(2z^3), \tag{20}$$

in the latter case. Further, on the basis of Eqs. (15) and (17), we can deduce that the value of the absorption

is the single-scattering contribution (e.g., [28]) to $J(\vec{0}, z)$ normalized to $J_b(\vec{0}, z)$. In Eq. (24b), as in Eq. (24a), the terms ($\propto k^{-2}w^{-2}$) describing the diffraction divergence effects can be neglected. Then, after

performing the integration and taking into account Eq. (24a), we obtain

$$\delta(z, \alpha_s, w, \gamma, g) = \alpha_s \gamma \sqrt{\frac{(w^2 + E^2)}{2(1-g)[\gamma^2 + 2(1-g)]}}$$
$$\times \; \text{arctg}\left\{\gamma z \sqrt{\frac{2(1-g)}{[\gamma^2 + 2(1-g)](w^2 + E^2)}}\right\}. \tag{25a}$$

The condition of neglecting the single-scattering contribution is obviously

$$\delta(z, \alpha_s, w, \gamma, g) \ll 1. \tag{25b}$$

This condition outlines a range of values of z, where the detected on-axis beam power decays exponentially due to absorption and scattering, that is [see also Eq. (24a)],

$$J(\vec{0}, z) = J_b \exp(-\alpha_t z). \tag{26}$$

As it is seen from relations (25a) and (25b), the extent of this range along axis $0z$ should decrease with increasing the medium turbidity ($\sim \alpha_s$). It is seen as well that, using Eq. (26), the value of the extinction coefficient α_t can be determined by exponential or log-linear fit of the data for $J(\vec{0}, z)$. Near the entrance of the laser beam into the turbid medium, in the limit $z \to 0$ or in practice when $z < (w^2 + E^2)^{1/2}$, from Eq. (25a), we obtain

$$\lim_{z \to 0} \delta(z, \alpha_s, w, \gamma, g) = \alpha_s z \gamma^2 / [\gamma^2 + 2(1-g)]. \tag{27}$$

At narrow angle of view of the optical detector, when $\gamma^2 \ll 2(1-g)$, according to Eq. (27), we have

$$\lim_{z \to 0} \delta(z, \alpha_s, w, \gamma, g) \cong \alpha_s z \gamma^2 / [2(1-g)] \ll \alpha_s z. \tag{27a}$$

In this case, Eq. (26) is in power down to the boundary $z = 0$ of the turbid medium. In the opposite case, when $\gamma^2 \gg 2(1-g)$, Eq. (27) is reduced to the form:

$$\lim_{z \to 0} \delta(z, \alpha_s, w, \gamma, g) \cong \alpha_s z. \tag{27b}$$

Then, instead of Eq. (24), we obtain:

$$J(\vec{0}, z) = J_b \exp(-\alpha_t z)(1 + \alpha_s z) \approx J_b \exp[-(\alpha_t - \alpha_s)z]$$
$$= J_b \exp(-\alpha_a z). \tag{28}$$

In this case, near the boundary the scattered light is entirely captured by the detector, and the decay with z of the detected light power is due to absorption alone. Similar slow-decay effect along with the exponential fall-off with decay constant α_t [Eq. (26)], at a maximum angle of acceptance $\gamma = \pi/2$, has also been found analytically and numerically, using different small-angle approaches [12, 14], and by simulations [22]. In the present work, the small-angle approximation allowed us to obtain analytically the true exponential fall-off laws $J(\vec{0}, z)$ obeys, Eqs. (26) and (28), the corresponding decay constants, α_t and α_a, and the corresponding conditions and ranges of validity, that is, the relations (25a, 25b), and $\gamma^2 \ll 2(1-g)$, in the former case, and $\gamma^2 \gg 2(1-g)$ and $z < (w^2 + E^2)^{1/2}$, in the latter case.

2.7 Expressions of $J(\vec{\rho}, z)$ and estimation of the optical parameters for Henyey–Greenstein indicatrix

The Henyey–Greenstein indicatrix is a more realistic characteristic of a scattering medium, taking into account the backscattering in the medium. The details about the derivation of the expressions of $J(\vec{\rho}, z)$ in this case are given in Appendix 1. The result obtained for the region of developed scattering ($\alpha_s z \gg 1$) is similar to that for Gaussian indicatrix [Eq. (11)]. The difference is that here

$$\chi = \alpha_{rs}(1 + g)/3 = \alpha_s(1 - g^2)/3 \tag{29}$$

and consequently

$$g = (1 - 3\chi/\alpha_s)^{1/2}, \tag{30}$$
$$\alpha_{rs} = \alpha_s(1 - g), \tag{31}$$

and

$$\alpha_s = \alpha_t - \alpha_a. \tag{32}$$

As in the case of Gaussian indicatrix, the values of α_a and α_t are determined by exponential or log-linear least-square fitting based on Eqs. (21) and (26), respectively.

2.8 Validity limits of the small-angle approach

The depths of validity z_V of the small-angle approach, along the laser-beam axis in the investigated medium, are estimated (in Appendix 2) to equal about several transport lengths, at strongly prevailing forward-peaked scattering. That is, $z_V \sim M \alpha_{rs}^{-1}$ where M is a number exceeding but of the order of unity. It is supposed as well there that when the deal of the backward scattering is noticeable, the depth of validity should be larger.

3 Experimental setup and procedures

The experimental arrangement for measuring the spatial distribution of the forward-propagating light power is represented in Fig. 1. A laser diode is used as near-infrared (NIR) light source emitting a nearly collimated continuous-wave optical beam of about 1 mm radius and wavelength $\lambda = 850$ nm. The total emitted light power can be varied from 20 to 50 mW. The turbid media investigated

experimentally are prepared by dilution of different amounts (from 17.5 to 433 ml) of Intralipid (IL)-20 % (Fresenius Kabi AB, Sweden) in 14 l distilled water placed in a plexiglass cubical container with 25 cm long sides. Correspondingly, the IL concentration varies from 0.0284 to 0.6822 %. We consider as IL concentration the volume fraction of soybean oil and egg lecithin forming the scattering submicron capsules in the dilution [29]. The volume fraction of these substances is 22.74 %, in stock Intralipid-20 %, and 11.952 %, in stock Intralipid-10 %.

The axis of the incident laser beam is perpendicular to the "frontal" wall of the container. It may be considered as oriented forward, in the direction of incidence of the beam, so coinciding with the axis $0z$ of the coordinate frame. As was mentioned above, the plane $z = 0$ is identified with the internal entry wall of the container filled with liquid turbid medium (see Fig. 1). The spatial distribution of the forward-propagating light power inside the container is measured by using a scanning optical fiber of 0.1 mm core diameter. The fiber is oriented antiparallel to the beam axis and is connected with an optical radiometer Rk-5100 (Laser precision corp., USA) with a RqP-546 silicon probe in external locking regime, 14 bits ADC, and a computer for appropriate data processing. The noise equivalent power (NEP) of the radiometer is 2×10^{-12} W. Its averaging (low-pass filtering) time constant τ_a may be set to 0.1, 1, or 10 s. To effectively damp down the signal fluctuations, the value of τ_a is chosen to be 1 s. By a transversal radial scan of the fiber at each stepwise-varied depth of interest and 400–800 averaged measurements per point, a set of data is obtained (the distribution of the received light power that is proportional to the light intensity) for any of the prepared turbid media. The corresponding on-axis detected power distributions are measured once more independently as well, by a longitudinal scan of the fiber along the beam axis. The scanning procedure in three mutually perpendicular (x, y, and z) directions is implemented by using three long travel stages Thorlabs LTS 300/M ensuring a minimum sampling step of 4 μm. The cross-sectional intensity distribution of the laser beam and the receiver directional diagram of the fiber in air have also been measured and shown to have approximately Gaussian shape [20]. The angle of view of the fiber in air is estimated to be $\gamma \sim 12°$, i.e., 0.21 rad. Then, its numerical aperture NA $= \sin \gamma \sim 0.21$. If the diluted Intralipid emulsion is considered as watery medium with refractive index $n \sim 1.34$, the angle of view of the fiber in these media will be $\gamma = \arcsin(\text{NA}/n) \sim 9°$, i.e., 0.16 rad. Thus, a spatial gating of the detected light power is realized within a solid angle of acceptance $\Omega = \pi\gamma^2 = 0.08$ sr and aperture area $A = \pi E^2 = 7.85 \times 10^{-9}$ m^2, where $E = 0.05$ mm.

The errors in the determination of the optical properties of turbid media, using the approach under consideration, may be conditioned by different factors. The experiments are conducted in dark laboratory at practically entirely removed influence of stray light. NEP of the radiometer is negligible as compared to the least measured power values of practical interest for the experiment. Then, the signal fluctuations should be due mainly to the signal-conditioned shot noise [30], to digitizing noise, to laser power fluctuations, and to fluctuations of the detected light power caused by the random walk of the particles within the scattering volume. The random motion of the scatterers leads to spatio-temporal fluctuations of their density and size distribution and so to fluctuations of the optical coefficients and the scattered power itself [see, e.g., Eq. (9)]. The analytical estimation of the intensity of the detected power fluctuations would require a separate profound investigation. In the experiments, using low-pass filtering with 1 s time constant and 400 measurements per point, the relative root-mean-square (rms) signal fluctuations are reduced to levels of 2–3 %, in the low-scattering zone, and 0.6–0.7 %, in the developed-scattering zone.

4 Analysis of the experimental results and determination of the optical properties of Intralipid dilutions

In-depth profiles of the on-axis measured forward-propagating light power at different IL concentrations are given in Fig. 2. As it is seen in the figure, each of these profiles exhibits a well-distinguishable initial exponential fall-off region, where $J(z)/J(z + \Delta z) = \exp(\alpha_t \Delta z) = \text{const}$; Δz is the sampling step. This is in fact the region of prevailing single-scattering, where the attenuation of the on-axis detected signal (proportional to the on-axis beam intensity) obeys the law of Bouguer–Lambert–Beer (BLB) [8, 30],
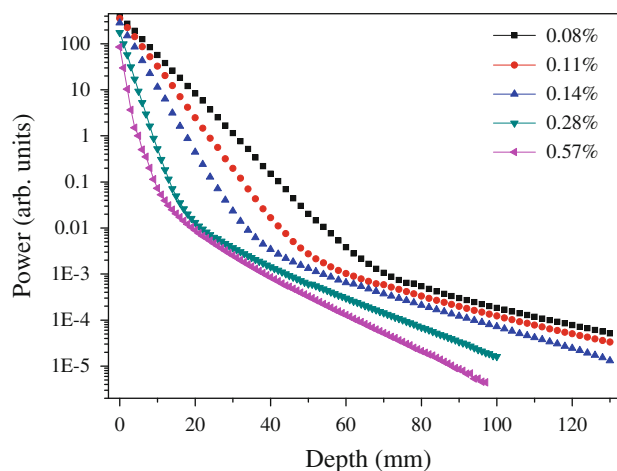

Fig. 2 In-depth profiles of the on-axis detected forward-propagating light power for different Intralipid concentrations

Table 1 Experimentally estimated values of the extinction coefficient for different Intralipid concentrations compared with the values of α_s according to van Staveren et al. [29]

Intralipid (%)	α_t (cm^{-1})	α_s [29] (cm^{-1})	Intralipid (%)	α_t (cm^{-1})	α_s [29] (cm^{-1})
0.028	0.690	0.561	0.284	5.890	5.613
0.057	1.250	1.122	0.313	6.470	6.174
0.085	1.935	1.684	0.341	6.860	6.735
0.114	2.500	2.245	0.398	7.730	7.858
0.142	3.150	2.863	0.455	8.651	8.980
0.171	3.728	3.368	0.512	9.350	10.103
0.199	4.350	3.929	0.568	10.240	11.225
0.227	4.920	4.490	0.682	11.600	13.470
0.256	5.410	5.051			

with decay constant α_t [see Eq. (26)]. The extent of this region decreases with the increase of the IL concentration [see also Eq. (25a) and inequality (25b)]. The exponential decay of the on-axis detected light power allows one to determine the extinction coefficient α_t by using loglinear least-squares fit. The estimated values of α_t, depending on the IL concentration, are given in Table 1 and represented graphically in Fig. 3. The relative error in the determination of α_t varies (increases) from 0.26 %, at IL concentration of 0.08, to 1.2 % at 0.68 % IL concentration. At 0.28 % IL concentration, the error is 0.4 %. The polynomial fit of the points given in this figure reveals a quadratic dependence of α_t on the IL concentration C defined in %. The fitting curve obtained without fixing its intercept (that is, α_t at zero IL concentration) has an intercept equal to 0.022 cm^{-1} with twice larger standard error. The published data for the absorption coefficient of pure water at $\lambda = 850$ nm (e.g., [31, 32]) vary from 0.041 to 0.043 cm^{-1}. The fitting curve shown in Fig. 3 is obtained at a fixed intercept of 0.043 cm^{-1}. For relatively low IL concentrations, including and below 0.2 %, the dependence of α_t on C is linear, which is in agreement with the results obtained formerly by us and other researchers [19–23]. There are no direct data in the literature about the extinction and scattering coefficients α_t and α_s of IL dilutions at $\lambda = 850$ nm. Nevertheless, by using different available empirical formulae and plots of α_t and α_s as functions of λ for some low-concentration dilutions of IL-10 % or IL-20 %, one may evaluate them at $\lambda = 850$ nm. Then, it is not difficult by linear extrapolation to estimate α_t or α_s of different-percentage Intralipid dilutions. For instance, the extinction coefficient of $\sim$0.6–0.7 % IL dilution is estimated on the basis of results from different works [26, 29, 33, 34] to be from 9 to 14 cm^{-1}. The result we have obtained here for 0.682 % IL dilution from IL-20 % is $\alpha_t = 11.6$ cm^{-1}. As a more concrete example, according to an empiric (substantiated by Mie-theory calculations) formula of van Staveren et al. [29] concerning the scattering coefficient of dilutions of Intralipid-10 %, $\alpha_s(\lambda)$ (mL^{-1}Lmm^{-1}) = 0.016 $\lambda^{-2.4}$ (μm) for 400 nm $< \lambda <$
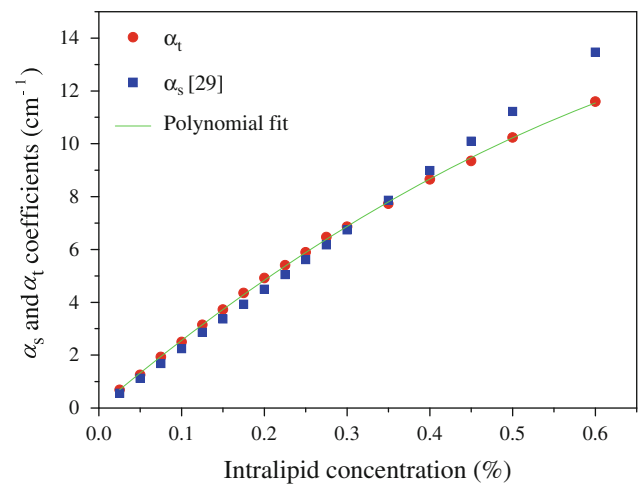

Fig. 3 Experimentally estimated values of the extinction coefficient α_t (*circles*) and values of α_s according to van Staveren et al. [29] (*squares*) versus Intralipid concentration. The *solid curve* represents a polynomial fit of the α_t data, with fixed intercept $\alpha_t(0) = 0.043$ cm^{-1}, revealing a quadratic dependence

1,000 nm, the value of α_s of 0.01195 % IL dilution at $\lambda = 850$ nm is 0.0236 mm^{-1}. Then, for 0.6 % IL concentration, we obtain $\alpha_s = 1.185$ mm^{-1} or 11.85 cm^{-1}. The results calculated in the same way for all the concentrations we have considered are given for comparison in Table 1 and Fig. 3. They are nearly below our results for α_t at lower concentrations.

The nonlinear behavior of α_t, seen in Fig. 3, is not unknown, at all. Similar dependence has been observed in [23], where the turbid media under investigation are low-concentration dilutions of milk. It is possibly the initial phase of the nonlinear dependence of α_s on C at higher IL concentrations (up to 25 %) observed by Zaccanti et al. [35] and analyzed and described theoretically by Giusto et al. [36]. Obviously, some more theoretical and experimental efforts are necessary here to understand entirely this problem. One should take into account the fact that above a characteristic concentration of the scattering substance, the distance between the neighboring effective scatterers
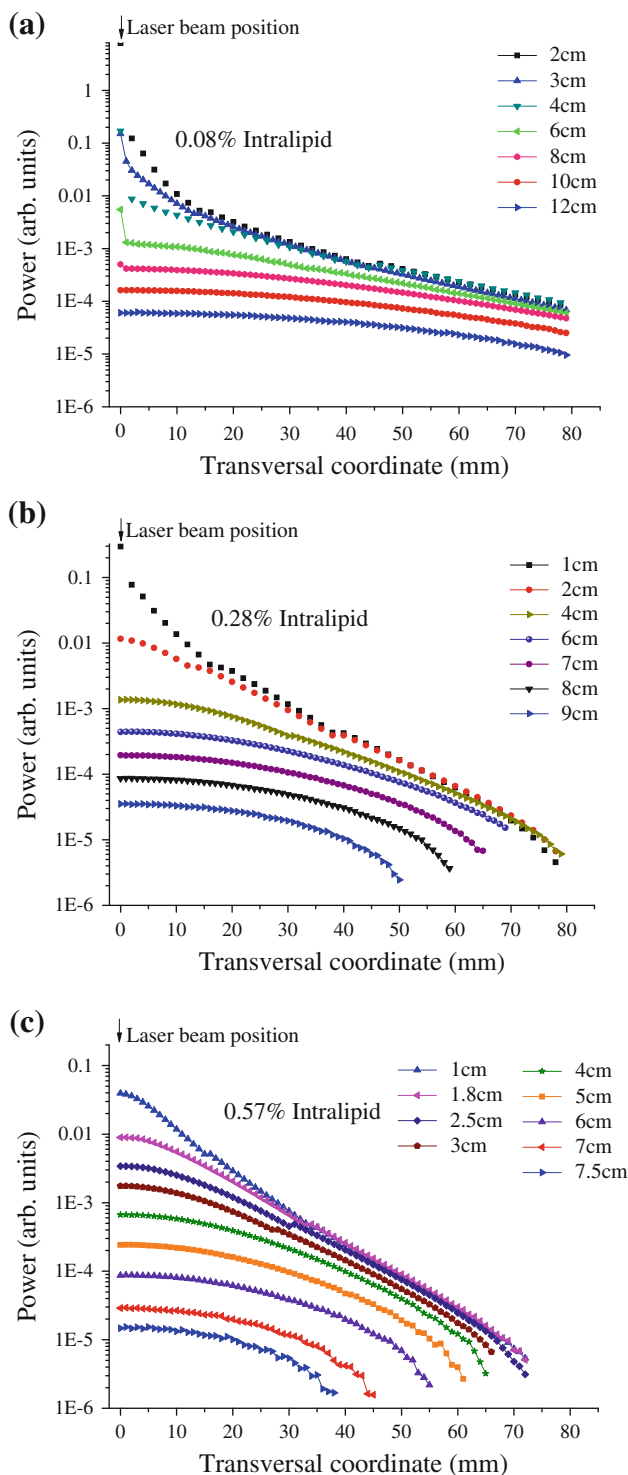
(a) 0.08% Intralipid

Legend: 2cm, 3cm, 4cm, 6cm, 8cm, 10cm, 12cm

(b) 0.28% Intralipid

Legend: 1cm, 2cm, 4cm, 6cm, 7cm, 8cm, 9cm

(c) 0.57% Intralipid

Legend: 1cm, 1.8cm, 2.5cm, 3cm, 4cm, 5cm, 6cm, 7cm, 7.5cm

Fig. 4 Transversal radial distributions of the detected forward-propagating light power at different depths and Intralipid concentrations

becomes comparable with their sizes and smaller than the wavelength λ of the laser radiation. For instance, as it is estimated in [29], at $\lambda = 1,100$ nm, the most effective Intralipid-10 % scatterers weighted in water (of 250 nm

diameter) have less than 3–4 particle-diameter (and one wavelength) spacing for IL-10 % concentrations above 4 %. In our notation here, this is a concentration $C = 0.48$ %. Then, the different scatterers would not act independently, but collectively, as packs of particles. The collective scattering effects should lead to violation of both the linearity of $\alpha_s (C)$ and the constancy of the g-factor (see also in [8, 35–40]).

As it is shown in Fig. 4, the transversal radial distributions of the detected power within the exponential fall-off (BLB) region (see also Fig. 2) consist of two components, the decaying unscattered light beam seen as a central peak and a pedestal of scattered light. A similar picture has been observed in [22]. The experimentally determined ratio $h(z) = J(0,z)/J(0,z + \Delta z)$ is shown in Fig. 5 as a function of z compared with the z-dependent quantities $h_1(z) = [(z + \Delta z)/z]^3$ and $h_2(z) = [(z + \Delta z)/z]^4$. It is seen that at each IL concentration, there exists an initial interval of depths where the function $h(z)$ fluctuates around a constant level $\sim \exp(\alpha_t \Delta z)$. The extent of this interval decreases with increasing the IL concentration and outlines the BLB region. For concentrations of 0.08, 0.28, and 0.57 %, the BLB-zone depths D_{BLB} are seen to be ~ 5 cm = 3.45 MFP, 0.7 cm = 4.12 MFP, and 0.3 cm = 3.08 MFP, respectively. The mean free paths of the photon MFP = α_t^{-1} and the quantities $\exp(\alpha_t \Delta z)$ are evaluated by using the data for α_t given in Table 1. As a whole, the results illustrated in Fig. 5 are in accordance with those illustrated in Figs. 2 and 4.

With increasing the depths in the dilutions, after passing a transient zone from low to developed scattering, a region of developed scattering is attained, where $\alpha_s z \gg 1$, the light beam consists of practically entirely scattered light, and the on-axis detected light power falls as z^{-4} rather than z^{-3}. Such developed-scattering regions are seen in Fig. 5, where, beginning from a depth D_{ds} depending on the IL concentration, the curve $h(z)$ becomes nearly coincident with $h_2(z)$. It is only slightly shifted above because in fact $J(0,z)/J(0,z + \Delta z) \cong [(z + \Delta z)/z]^4 \exp(\alpha_a \Delta z)$ [see Eq. (15)]. According to Fig. 5, for IL concentrations of 0.08, 0.28, and 0.57 %, the developed-scattering zones begin, respectively, at depths D_{ds} of ~ 9, 3.5, and 3 cm. The corresponding optical depths $\alpha_t z$ ($\approx \alpha_s z$), evaluated by using the data for α_t given in Table 1, are ~ 12, 20, and 30. The transverse radial distributions of the detected power have already bell-shaped, like Gaussian forms (seen in Figs. 4, 6, and also in [22]) whose e^{-1} half-width $w(z)$ increases with z nearly as $z^{3/2}$ [Eq. (16)]. The experimental determination of $w(z)$ based on Gaussian fitting of the transversal distribution allows one to determine the parameter χ, using the relation (16). The relative errors in
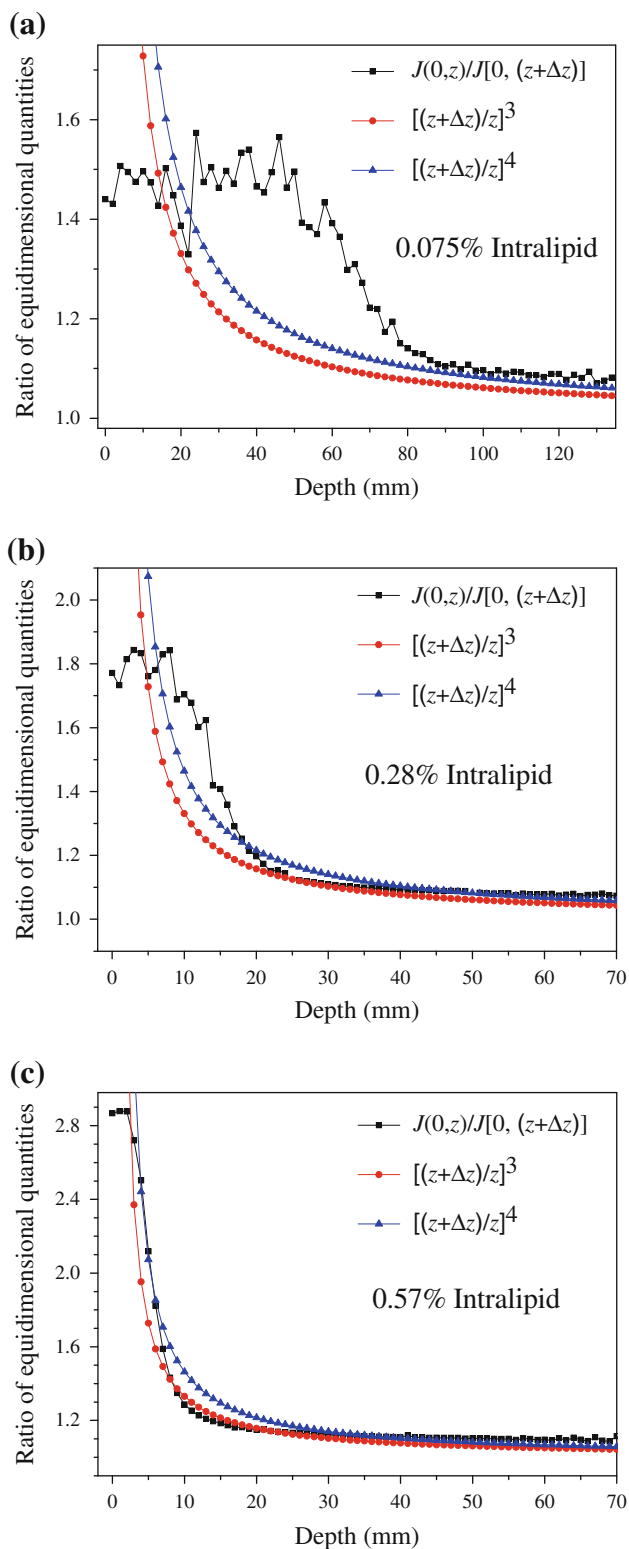
(a)

(b)

(c)

Fig. 5 Dependences $J(0,z)/J(0,z + \Delta z)$ compared with the quantities $[(z + \Delta z)/z]^3$ and $[(z + \Delta z)/z]^4$ at different Intralipid concentrations; the sampling step $\Delta z = 2$ mm (**a**) and 1 mm (**b, c**)
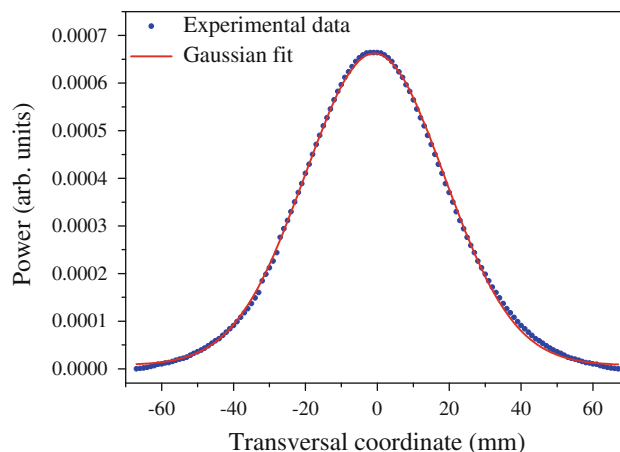

Fig. 6 Transversal radial distribution of the detected forward-propagating light power (for IL concentration of 0.568 % and depth of 4 cm) fitted by a Gaussian curve

the determination of $w(z)$ are below 1 %. The corresponding $\chi(z)$ determination errors are twice larger. To reduce the influence of additional implicit fluctuation factors, the final estimates of χ are obtained as the arithmetic mean of the results from 3 to 4 successive depths with spacing of 0.5 or 0.4 cm within the region of developed scattering. The rms deviations of these estimates are also evaluated. Then, on the basis of Eqs. (19), (21), (23), (30), and (31), at known α_t and negligible α_a, the values of α_{rs} and g are estimated for both Gaussian and Henyey–Greenstein indicatrices. In practice, to obtain the estimates of α_{rs} and g given in Table 2, instead of α_s, the values of α_t given in Table 1 have been used. The uncertainties in the determination of α_{rs} and g (Table 2) are evaluated by linear error transfer. The depths z employed for estimation of α_{rs} and g have been chosen to be consistent with the conditions $\alpha_s z \gg 1$, $z > D_{ds}$, and $\alpha_{rs} z < M$ [according to relation 42]. Those results for $w(z)$ have been used as well which closely satisfy the criterion $[w(z_1)/w(z_2)]^2 = (z_1/z_2)^3$ following from Eq. (19). The maximum-used-depth values of $\alpha_{rs} z$ have been a posteriori established (at already estimated α_{rs}) to be about 2–3 and 3–5, respectively, for Gaussian and Henyey–Greenstein indicatrices. So, one may conditionally assume that the corresponding depths of validity, $z_V \sim M\alpha_{rs}^{-1}$, of the small-angle approximation for both the indicatrices are determined by the values of $M = 3$ and 5. Then, e.g., at IL concentrations $C = 0.085$ and 0.284 %, using the data given in Table 2, we obtain that $z_V \sim 15$ and 5 cm, respectively. The corresponding intervals of depths of interest, $z \in [D_{ds}, z_V]$, are from 9 to 15 cm, at $C = 0.085$ %, and from 3.5 to 5 cm, at $C = 0.284$ %. The above example illustrates the tendency to narrowing and shifting left the intervals $[D_{ds}, z_V]$ with increasing the

Table 2 Experimentally estimated values of the reduced-scattering coefficient and the anisotropy factor for different Intralipid concentrations

Intralipid (%)	0.085	0.114	0.142	0.284
α_{rs} Gauss (cm^{-1})	0.200 ± 0.004	0.264 ± 0.009	0.338 ± 0.028	0.640 ± 0.009
α_{rs} H–G (cm^{-1})	0.327 ± 0.007	0.435 ± 0.015	0.558 ± 0.050	1.054 ± 0.017
g Gauss	0.897 ± 0.002	0.894 ± 0.003	0.893 ± 0.009	0.891 ± 0.002
g H–G	0.831 ± 0.004	0.826 ± 0.006	0.823 ± 0.016	0.821 ± 0.003

concentration C. Note as well that the estimated values of $z_V \sim 3\,\alpha_{rs}^{-1}$ and $5\alpha_{rs}^{-1}$ are nearly around the lower limit, $z_{ld} \sim 4\alpha_{rs}^{-1}$, of the diffusive regime of light propagation as it is defined in Ref. [8] on the basis of comparison between results of analytical diffusion-approach-based investigations and Monte Carlo simulations. Results for $w(z)$ and χ and respectively for α_{rs} and g are obtainable at relatively low IL concentration of 0.0853, 0.1137, 0.1421, and 0.2842 % (Table 2). The values obtained of the g-factor for Gaussian and Henyey–Greenstein indicatrices are respectively ~ 0.89 and 0.82. These values differ significantly from that, $g = 0.607$ for $\lambda = 850$ nm, predicted by another empiric formula of van Staveren et al. [29] for Intralipid-10 %, $g(\lambda) = 1.1$–$0.58\,\lambda$ (µm). At the same time, the anisotropy factor obtained here for Henyey–Greenstein indicatrix is very near the one, $g \sim 0.79$ at $\lambda = 850$ nm, we have deduced from Ref. [33], where a graphical dependence of $g(\lambda)$ is obtained by processing data for $\alpha_t \approx \alpha_s$ and α_s of stock Intralipid-10 % measured, respectively, using the approaches of narrow beam attenuation and diffuse reflectance from a semi-infinite medium. The same result, $g = 0.79$ at $\lambda = 850$ nm, is obtained by using the formula $g(\lambda) = 2.25\,\lambda^{-0.155}$ (µm) [41] approximating analytically the above-mentioned graphical dependence of g on λ. Although the value of $g \sim 0.79$ is out of the error intervals around our results (see Table 2), the difference of 3.7 % indicates a close proximity between both the results.

At last, we have also estimated the values of α_a for IL concentrations of 0.085 and 0.114 %, using log-linear fit of each of the rectilinear regions, shown in Fig. 7, of the dependence $y_1(z) = \ln[J(\vec{0}, z)z^4]$ [see Eqs. (15) and (21)]. At lower concentrations, the rectilinear regions are at depths exceeding the range of the data obtained. Then, to observe these regions, one should use more powerful laser sources. At higher concentrations, the rectilinear regions are too narrow and not clearly identifiable. The values we have obtained at both the concentrations of concern are (0.067 ± 0.001) and (0.083 ± 0.002) cm^{-1}, respectively, with ~ 2 % relative error. The corresponding values, (0.024 ± 0.001) and (0.040 ± 0.002) cm^{-1}, corrected for the absorption of water at $\lambda = 850$ nm, are of the order of that, 0.054 cm^{-1}, obtained in Ref. [42] at $\lambda = 1{,}064$ nm and $C = 0.1195$ % by processing data from diffuse
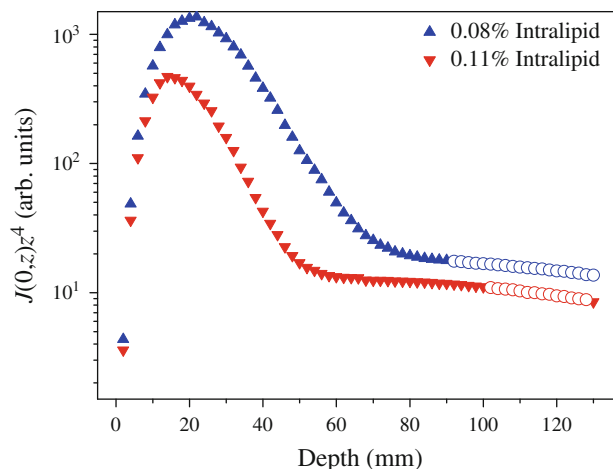

Fig. 7 Illustration of the dependences $y_1(z) = \ln[J(\vec{0}, z)z^4]$ for two Intralipid concentrations. *Open circles* denote the rectilinear regions used for estimation of the values of α_a

reflectance and transmission measurements and collimated transmission measurements. Using the obtained values of α_a and the corresponding quantities of α_t and α_{rs} given, respectively, in Tables 1, 2, according to Eqs. (23), and (32), and (30) (with $\chi = \alpha_{rsG}$), we obtain again that $g_G \sim 0.89$ and $g_{HG} \sim 0.82$ at $C = 0.085$ or 0.114 %.

5 Summary

The results obtained in this work show that in general, the small-angle approximation could adequately describe the propagation of laser radiation through turbid media. The depth of validity of this approximation, z_V, is shown to be of the order of the transport mean free path of the photon in the medium of interest. That is, $z_V \sim M\alpha_{rs}^{-1}$ where M is a number exceeding but of the order of unity. The values of M for IL dilutions of relatively low concentrations $C \leq 0.3$ %, having Gaussian or Henyey–Greenstein indicatrices, are estimated experimentally to be ~ 3 or 5, respectively. The corresponding depths $z_V \sim 3\alpha_{rs}^{-1}$ or $5\alpha_{rs}^{-1}$ are of the order of the lower limit, $z_{ld} \sim 4\alpha_{rs}^{-1}$, of the region of diffusive propagation of light [8]. It is also shown theoretically that at optical depths $\alpha_s z$ of the order of unity or smaller, in the region of low scattering, where the

forward light flow consists of mainly unscattered and single-scattered components, the on-axis detected forward-propagating light power behaves in two ways. When the receiver angle of view γ is less than the characteristic angle of scattering $\sim [2(1-g)]^{1/2}$, the detected power $J(\vec{0}, z)$ decreases with z exponentially, with decay constant α_t. In the opposite case, one more exponential fall-off region exists near the entry wall of the container, for $z < (w^2 + E^2)^{1/2}$. The decay constant in this case is α_a. For large optical depths ($\alpha_s z \gg 1$), in the region of developed scattering, where the multiple-scattered light is prevailing and the relation $D_{ds} < z < z_V$ holds, it is obtained that $J(\vec{0}, z) \propto z^{-3}$ or z^{-4} when $\gamma^2 \gg \chi z$ or $\gamma^2 \ll \chi z$, respectively (Sect. 2). The theoretical analysis of the transverse radial distribution of the detected forward-propagating light power in this region shows that it should have Gaussian shape with e^{-1} half-width $w(z) \propto z^{3/2}$. As a whole, the obtained theoretical results are in agreement with results obtained by other researchers experimentally [22, 23], by simulations [22], or using other theoretical approaches [12, 14, 15, 18]. The analytical expressions obtained in the work about the spatial distribution of the detected light power allow one in principle to estimate, on the basis of the experimental data, the values of α_t, α_a, α_{rs}, and g for both the indicatrices under consideration.

The experimental results confirm in general the theoretical predictions. The exponential fall-off regions with decay constant α_t [here $\gamma^2 < 2(1-g)$] are clearly identified (Fig. 2) and used for determination of the values of α_t at different IL concentrations C (Fig. 3). The dependence $\alpha_t(C)$ is shown to be nonlinear (quadratic) in general, but at low concentrations ($C < 0.3$ %), it is practically linear and closely describes the data obtained by linear extrapolation of results of van Staveren et al. [29] concerning dilutions of Intralipid-10 % at $\lambda = 850$ nm. The near coincidence between the experimentally estimated values of α_t and the extrapolated values of α_s at low IL concentrations is indirect confirmation of the validity of the formula of van Staveren et al. [29] (see above) about the dependence of α_s on λ of dilutions of Intralipid-10 %. At large optical depths, within the interval $D_{ds} < z < z_V$, the on-axis detected light power $J(\vec{0}, z)$ turns out to behave as nearly z^{-4} rather than z^{-3} (Fig. 5). The transverse radial distribution of the forward-propagating light intensity has Gaussian-like shape (Fig. 6) with e^{-1} half-width $w(z)$. We have used the value of $w(z)$ to estimate the reduced-scattering coefficient α_{rs} and the anisotropy factor g of dilutions of low (~ 0.085–0.284 %) IL concentrations. It is found, in particular, that the g-factor is ~ 0.89 for Gaussian indicatrix and ~ 0.82 for Henyey–Greenstein indicatrix. The result obtained for Henyey–Greenstein indicatrix is near that, $g = 0.79$ at $\lambda = 850$ nm, evaluated using a

dependence of g on λ obtained empirically by Flock et al. [33] and Jacques [41]. The values of the absorption coefficient of the IL component in dilutions of low concentrations (0.085 and 0.114 %), obtained by using log-linear least-squares fit of the dependence $J(\vec{0}, z)z^4$ in its rectilinear zone as well as correction for the absorption of water, are of the order of that obtained in [42] at $\lambda = 1,064$ nm.

The investigations performed in the work are important for the development of methods for measuring the optical characteristics of turbid media such as tissues and experimental tissue-like phantoms. They would also be useful in the process of establishing the laws governing the radiative transfer inside the optically investigated biological objects. The further work on the subject will be directed to increasing the experimental accuracy and refining the theoretical models as well as to experimenting with Intralipid-10 % and using shorter and longer-wavelength laser radiation.

Appendix 1: Estimation of $J(\vec{\rho}, z)$ for Henyey–Greenstein indicatrix

Using Eqs. (4) and (8c), for Henyey–Greenstein indicatrix, we obtain

$$
\begin{aligned}
\tilde{i}(\vec{q} + \vec{\kappa}z') &\cong [(1-g^2)/4\pi] \int\limits_{4\pi} \mu d\omega \exp[j\vec{s}_\perp \cdot (\vec{q} + \vec{\kappa}z')] \\
&\quad (1 + g^2 - 2g\mu)^{-3/2} \\
&\cong [(1-g^2)/2] \int\limits_{-1}^{1} d\mu J_0[\sqrt{1-\mu^2}Q(z')] \\
&\quad (1 + g^2 - 2g\mu)^{-3/2},
\end{aligned}
\tag{33}
$$

where J_0 is Bessel function of the first kind, zero order, and $Q(z') = |\vec{q} + \vec{\kappa}z'|$. When deriving the relations (33), we assumed that the indicatrix is sharply forward peaked, the scattered light is mainly forward directed, and $\int_{-\infty}^{+\infty} d\vec{s}_\perp = \int_{4\pi} \mu d\omega \approx \int_{4\pi} d\omega$ [13]. When $\alpha_s z \gg 1$, as in the case of Gaussian indicatrix, the integrand contribution to the integral in Eq. (9) is essential for values of $\tilde{i}$ near unity, that is, for $|\vec{q} + \vec{\kappa}z'| \ll 1$. Then, the function J_0 is expressible asymptotically as $J_0\left[\sqrt{1-\mu^2}Q(z')\right] \cong 1 -(1/4)(1-\mu^2)Q^2(z')$. This approximation of J_0 permits one to perform integration over μ in (33). The result is

$$\tilde{i}(\vec{q} + \vec{\kappa}z') \cong 1 - [(1-g)(\vec{q} + \vec{\kappa}z')^2/2](1+g)/3. \quad (34)$$

Using this expression of $\tilde{i}$ in Eq. (9), we obtain for $J(\vec{\rho}, z)$ the expression of Eq. (11) with χ given by Eq. (29).

When $\alpha_s z$ is of the order of unity or smaller, it is difficult to perform detailed analytical estimation of the on-axis detected light power $J(\vec{0}, z)$ for Henyey–Greenstein indicatrix. In this case, a general estimation could be conducted that is valid for any type of indicatrix. Let us first suppose that $(w^2 + E^2)^{1/2}/2 > z$ and $\gamma/2 > [2(1-g)]^{1/2}$. Then, the value of the integral in Eq. (9) is determined by the exponential terms in the integrand containing κ^2 and q^2. The contribution to the integral is essential for $\kappa < 2/(w^2 + E^2)^{1/2} < 1/z$ and $q < 2/\gamma < [2(1-g)]^{-1/2} \sim 1$, that is, $\kappa z \ll 1$ and $q \ll 1$. For such values of κ and q, according to Eq. (8c) [see also Eqs. (10a) and (33)], $\tilde{i}(\vec{q} + \vec{\kappa}z') \approx 1$. Then, from Eq. (9), we obtain Eq. (28) for $J(\vec{0}, z)$.

Suppose further that $\gamma/2 \ll 1$. In this case, the essential interval of integration over $\vec{q}$ involves mostly values of $q \gg 1$. For $q \gg 1$, because of strong oscillations of the integrand in Eq. (8c), $\tilde{i}(\vec{q} + \vec{\kappa}z') \ll 1$ [see also Eqs. (10a) and (33)]. Thus, on the average, the integral exponential term in Eq. (9) is expressible as

$$\alpha_t \int_0^z dz'[1 - W_0\tilde{i}(\vec{q} + \vec{\kappa}z')] = (\alpha_t - \alpha_s\xi)z, \quad (35)$$

where $\xi = z^{-1}\int_0^z dz'\tilde{i}(\vec{q} + \vec{\kappa}z') \ll 1$. Taking into account the expression of Eq. (35) in Eq. (9) and neglecting the term $\alpha_s\xi z$, we obtain Eq. (26) for $J(\vec{0}, z)$.

Appendix 2: Estimation of the depth of validity of the small-angle approximation

At negligible backscattering that is intrinsic to a Gaussian indicatrix, an estimate of the in-depth validity limit of the small-angle approach can be obtained, considering a "mean photon" that undergoes forward-peaked scattering in one only plane containing the beam axis. At each, independent, m-th act of scattering the photon changes its direction of propagation with angle γ_m. After N scattering events, the resultant angle of propagation with respect to the beam axis will be $\gamma_r = \gamma_1 + \gamma_2 + \cdots \gamma_N$. Then, the mean-square angular deviation from the beam axis is

$$\langle \gamma_r^2 \rangle = N\sigma_\gamma^2, \quad (36)$$

where
$\sigma_\gamma^2 = \langle \gamma_1^2 \rangle = \langle \gamma_2^2 \rangle = \cdots = \langle \gamma_N^2 \rangle = 2\pi \int_0^\infty ds_\perp i(s_\perp)s_\perp^3$. At the same time, the photon reaches an average depth (e.g., [8])

$$z = \alpha_s^{-1}(1 - g^N)/(1 - g). \quad (37)$$

From Eq. (37), we obtain that

$$N = \ln(1 - \alpha_{rs}z)/\ln g. \quad (38)$$

When $g \sim 1$, most frequently $\gamma_m \ll 1$ and $\gamma_m^2 \cong 2(1 - \cos\gamma_m)$. Correspondingly,

$$\sigma_\gamma^2 = \langle \gamma_m^2 \rangle \cong 2(1 - \langle \cos\gamma_m \rangle) = 2(1 - g). \quad (39)$$

Taking into account relations (38) and (39) in Eq. (36), we obtain

$$\langle \gamma_r^2 \rangle \cong 2(1 - g)\ln(1 - \alpha_{rs}z)/\ln g. \quad (40)$$

For the small-angle approximation to be in power, one may require that $\langle \gamma_r^2 \rangle^{1/2} < \pi/2$ or $\langle \gamma_r^2 \rangle < \pi^2/4$, which leads [see Eq. (40)] to the condition

$$z < \alpha_{rs}^{-1}\left[1 - g^{\frac{\pi^2}{8(1-g)}}\right] \sim \alpha_{rs}^{-1}. \quad (41)$$

In other words, the depth of validity $z = z_V$ should not exceed the transport mean free path α_{rs}^{-1}. Such a condition is in agreement with the interpretation of α_{rs}^{-1}, given in [8], as "the mean distance traveled by photons along the initial direction of propagation before they have effectively 'forgotten' their original direction of motion." As the obtained value of $z_V \sim \alpha_{rs}^{-1}$ is conditioned by the rms value of γ_r, it may be considered as a lower estimate of the depth of validity. Then, a more realistic definition of z_V would be that

$$z_V \sim M\alpha_{rs}^{-1}, \quad (42)$$

where M is a number exceeding but of the order of unity.

When the backscattering cannot be neglected as it is in the case of Henyey–Greenstein indicatrix, the acts of forward scattering will not be so frequent and the small-angle forward propagation will continue to longer distances in the medium. In addition, the e^{-1} forward angular width of Henyey–Greenstein indicatrix is $[(1-g)/(2g)]^{1/2}$ times smaller than that of Gaussian indicatrix. Thus, one may expect that in the case of indicatrix of Henyey–Greenstein, the depth of validity of the small-angle approximation should be larger.

Appendix 3: Expression of the radiance $I(\vec{r}; \vec{s})$ for Gaussian indicatrix, in the developed-scattering zone ($\alpha_s z \gg 1$)

Using in Eq. (8) the relations (3), (6), (8a–8c), and the asymptotic representation (10b) of the Gaussian indicatrix Fourier transform, we can perform analytical integration and obtain the following expression of $I(\vec{r}; \vec{s})$ valid for $\alpha_s z \gg 1$:

$$I(\vec{r};\vec{s}) = I(\vec{\rho},\vec{z};\vec{s}_\perp) = \left\{ P_t / [\pi^2 \xi(z)\zeta(z)] \right\} \exp(-\alpha_a z)$$
$$\times \exp\left\{ -\rho^2/\xi(z) - [\vec{\rho}\alpha_{rs}z^2/\xi(z) - \vec{s}_\perp]^2/\zeta(z) \right\},$$
$$(43)$$

where $\xi(z) = w^2 + (2/3)\alpha_{rs}z^3$, and $\zeta(z) = (\text{kw})^{-2} + (2w^2\alpha_{rs}z + \alpha_{rs}^2 z^4/3)/\xi(z)$. Under the assumption that $(\text{kw})^{-2} \to 0$, and $w^2 \ll \alpha_{rs}z^3$, Eq. (43) is reduced to the form

$$I(\vec{r};\vec{s}) = [3P_t/(\pi^2\alpha_{rs}^2 z^4)] \exp(-\alpha_a z)$$
$$\times \exp\left\{ -[6/(\alpha_{rs}z^3)](\rho^2 - z\vec{\rho}\cdot\vec{s} + z^2 s_\perp^2/3) \right\}. \quad (44)$$

Further, we may represent α_{rs} in the form $\alpha_{rs} = \alpha_s(1-g) = <\theta_1^2>/(2d_0)$, where $d_0 = \alpha_s^{-1}$ is the mean free path of the photon between two successive acts of scattering, and $<\theta_1^2> = \sigma_\gamma^2 = 2(1-g)$ [see in [18] and Eq. 39]. Then, using in Eq. (44) the above representation of α_{rs} and normalizing $I(\vec{r};\vec{s})$ by the quantity $\int I(\vec{r};\vec{s})\mathrm{d}\vec{\rho}\mathrm{d}\vec{s}_\perp = P_t \exp(-\alpha_a z)$, we attain just the small-angle approximation result given in [18] for the probability density distribution that an energy unit (say photon) propagating initially along axis $0z$ will pass a plane $z = \text{const}$ through a surface element $\mathrm{d}x\mathrm{d}y$ around a point (x,y), within an infinitesimal cone around a direction $\vec{s}$. This result is obtained as a solution of a Fokker–Planck type diffusion equation approximating the transfer equation. The boundary/initial condition considered at the plane $z = 0$ is as if implying a point source of unity power emitting photons along axis $0z$. A physically more realistic picture, however, leading to the same solution, is an incident (along $0z$) collimated Gaussian laser beam whose radius w tends to a "physical zero" exceeding essentially λ. That is, the relation $(\text{kw})^{-2} \ll 1$ remains in power. Note as well that, according to Eq. (8c), independent of the concrete form of $i(s_\perp)$, the Taylor series expansion of $\tilde{i}(\vec{q})$ including the first two terms is

$$\tilde{i}(\vec{q}) = 1 - \sigma_\gamma^2 q^2/4 \quad (45)$$

(see also Sect. 2.6). Then, if we use in Eq. (8) the expression (45) of $\tilde{i}(\vec{q})$ instead of (10b), we shall obtain Eqs. (43), and (44) in the "physical limit $w \to 0$" (see above), with $\alpha_{rs} = \sigma_\gamma^2/2d_0$. Eq. (44) with $\alpha_{rs} = \sigma_\gamma^2/2d_0$ and $P_t = 1$ is obtained also in Ref. [15] by using path integral technique to solve the radiative transfer equation under the boundary condition of Ref. [16] and the assumption that $\tilde{i}(\vec{q})$ is given by Eq. (45).

References

1. S. Fantini, S.A. Walker, M.A. Franceschini, M. Kaschke, P.M. Schlag, K.T. Moesta, Appl. Opt. **37**, 1982–1989 (1998)
2. A.H. Hielscher, A.Y. Bluestone, G.S. Abdoulaev, A.D. Klose, J. Lasker, M. Stewart, U. Netz, J. Beuthan, Dis. Markers **18**, 313–337 (2002)
3. D. Grosenick, K.T. Moesta, H. Wabnitz, J. Mucke, C. Stroszczynski, R. Macdonald, P.M. Schlag, H. Rinneberg, Appl. Opt. **42**, 3170–3186 (2003)
4. A.P. Gibson, J.C. Hebden, S.R. Arridge, Phys. Med. Biol. **50**, R1–R43 (2005)
5. W. Drexler, J.G. Fujimoto, *Optical Coherence Tomography: Technology and Applications* (Springer, Berlin, 2008)
6. P. Taroni, A. Pifferi, G. Quarto, L. Spinelli, A. Torricelli, F. Abbate, A. Villa, N. Balestreri, S. Menna, E. Cassano, R. Cubeddua, J. Biomed. Opt. **15**, 060501 (2010)
7. A. Ishimaru, *Wave Propagation and Scattering in Random Media*, vol. 1 (Academic Press, New York, 1978)
8. F. Martelli, S. Del Bianco, A. Ismaelli, G. Zaccanti, *Light Propagation Through Biological Tissue and Other Diffusive Media: Theory, Solutions, and Software* (SPIE Press, Bellingham, WA, 2010)
9. W.F. Cheong, S.A. Prahl, A.J. Welch, IEEE J. Quantum Electron. **26**, 2166–2185 (1990)
10. V. Tuchin, *Handbook of Optical Biomedical Diagnostics* (SPIE Press, Bellingham, WA, 2002)
11. L. Dolin, Radiophysics **7**, 380–382 (1964)
12. L. Dolin, Radiophysics **9**, 61–71 (1966)
13. L.S. Dolin, Izv. Atm. Ocean. Phys. **16**, 34–39 (1980)
14. R. Fante, IEEE Antennas Propag. Soc. AP **21**, 750–755 (1973)
15. J. Tessendorf, Phys. Rev. A **35**, 872–878 (1987)
16. L.T. Perelman, J. Wu, Y. Wang, I. Itzkan, R.R. Dasari, M.S. Feld, Phys. Rev. E **51**, 6134–6141 (1995)
17. S. Premoze, M. Ashikhmin, P. Shirley, in EGSR '03: Proceedings of the 14th Eurographics Symposium on Rendering, Aire-la-Ville, Switzerland, pp. 52–63 (2003)
18. H. Bremmer, Random volume scattering. Radio Sci. J. Res. **680**, 967–981 (1964)
19. L. Gurdev, I. Bliznakova, T. Dreischuh, O. Vankov, D. Stoyanov, L. Avramov, AIP Conf. Proc. **1203**, 716–721 (2009)
20. I. Bliznakova, L. Gurdev, T. Dreischuh, O. Vankov, D. Stoyanov, L. Avramov, Proc. SPIE **7747**, 774710 (2011)
21. L. Gurdev, T. Dreischuh, I. Bliznakova, O. Vankov, L. Avramov, D. Stoyanov, Phys. Scr. **2012**(T149), 014074 (2012)
22. S.D. Campbell, A. O'Connel, S. Menon, Q. Su, R. Grobe, Phys. Rev. E **74**, 061909 (2006)
23. S.D. Campbell, S. Menon, G. Rutherford, Q. Su, R. Grobe, Laser Phys. **17**, 117–123 (2007)
24. R. Marchesini, A. Bertoni, S. Andreola, E. Melloni, A. Sichirollo, Appl. Opt. **28**, 2318–2324 (1989)
25. P. Parsa, S. Jacques, N. Nishioka, Appl. Opt. **28**, 2325–2330 (1989)
26. R. Michels, F. Foschum, A. Kienle, Opt. Express **16**, 5907–5925 (2008)
27. L.G. Henyey, J.L. Greenstein, Astrophys. J. **93**, 70–83 (1941)
28. A. Deepak, U.O. Farrukh, A. Zardecki, Appl. Opt. **21**, 439–447 (1982)
29. H.J. van Staveren, C.J.M. Moes, J. van Marie, S.A. Prahl, M.J.C. van Gemert, Appl. Opt. **30**, 4507–4514 (1991)

30. R.M. Measures, *Laser Remote Sensing: Fundamentals and Applications* (Wiley, New York, 1984)
31. W.M. Irvine, J.B. Pollack, Icarus **8**, 324–360 (1968)
32. G.M. Hale, M.R. Querry, Appl. Opt. **12**, 555–563 (1973)
33. S.T. Flock, S.L. Jacques, B.C. Wilson, W.M. Star, M.J.C. van Gemert, Lasers Surg. Med. **12**, 510–519 (1992)
34. C. Chen, J.Q. Lu, H. Ding, K.M. Jacobs, Y. Du, X.-H. Hu, Opt. Express **14**, 7420–7435 (2006)
35. G. Zaccanti, S. Bianco, F. Martelli, Appl. Opt. **42**, 4023–4030 (2003)
36. A. Giusto, R. Saija, M.A. Iatì, P. Denti, F. Borghese, O.I. Sindoni, Appl. Opt. **42**, 4375–4380 (2003)
37. S.M. Rytov, Yu.A. Kravtsov, V.I. Tatarsky, *Introduction to Statistical Radiophysics, Part II, Random Fields* (Nauka, Moscow, 1978)
38. V. Twersky, J. Acoust. Soc. Am. **64**, 1710–1719 (1978)
39. V. Twersky, JOSA **69**, 1567–1572 (1979)
40. A. Isimaru, Y. Kuga, JOSA **72**, 1317–1320 (1982)
41. S. Jacques, Optical properties of Intralipid, an aqueous suspension of lipid droplets, Or. Med. Laser Cent. (1998), available online at http://omlc.ogi.edu/spectra/intralipid/
42. D.D. Royston, R.S. Poston, S.A. Prahl, J. Biomed. Opt. **1**, 110–116 (1996)